RSC Advances

PAPER

View Article Online
View Journal | View Issue

Cite this: *RSC Adv.*, 2020, **10**, 28674

The geometrical structure and electronic properties of trivalent Ho^{3+} doped Y_2O_3 crystals: a first-principles study

Meng Ju,[ab] Lu Pan,[a] Chuanzhao Zhang,[*b] Yuanyuan Jin,[b] Mingmin Zhong,[*a] Song Li,[b] Shichang Li,[c] Tie Yang[a] and Xiaotian Wang[*a]

Trivalent rare-earth holmium ion (Ho^{3+}) doped yttrium oxide (Y_2O_3) has attracted great research interest owing to its unique optoelectronic properties and excellent performances in many new-type laser devices. But the crystal structures of the Ho^{3+}-doped Y_2O_3 system (Y_2O_3 : Ho) are still unclear. Here, we have carried out a first-principle study on the structural evolution of the trivalent Ho^{3+} doped Y_2O_3 by using the CALYPSO structure search method. The results indicate that the lowest-energy structure of Ho^{3+}-doped Y_2O_3 possesses a standardized monoclinic *P*2 phase. It is found that the doped Ho^{3+} ion are likely to occupy the sites of Y^{3+} in the host crystal lattice, forming the $[HoO_6]^{9-}$ local structure with C_2 site symmetry. Electronic structure calculations reveal that the band gap value of Ho^{3+}-doped Y_2O_3 is approximately 4.27 eV, suggesting the insulating character of Y_2O_3 : Ho system. These findings could provide fundamental insights to understand the atomic interactions in crystals as well as the information of electronic properties for other rare-earth-doped materials.

Received 12th June 2020
Accepted 29th July 2020

DOI: 10.1039/d0ra05188h

rsc.li/rsc-advances

1. Introduction

Rare-earth (RE) doped laser materials have attracted enormous interests because of their abundant transition channels and sharp luminescence bands.[1–5] The potential applications have been widely investigated in a diversity of fields, such as optical imaging, quantum cascade lasers, high-density optical data storage and biophotonic areas.[6–9] A recent study reveals that the directly pumped Ho^{3+}-doped silica microsphere may be an excellent candidate for fabricating 2 μm laser, which can serve as laser-emitting source for mid-infrared telecommunications.[10]

Trivalent holmium ion ($4f^{10}$ configuration) is a greatly promising laser ion due to the substantial transition channels at various wavelengths in the UV, visible and infrared regions.[11,12] A well-known emission transition $^5I_7 \rightarrow {}^5I_8$ with wavelength near 2 μm of Ho^{3+} can serve as the so called "eye safe" solid-state laser system.[13] Yttrium oxide (Y_2O_3) is a typical cubic phase crystal structure with $Ia\bar{3}$ space group, which possesses low phonon energy and desirable physical properties including low thermal expansion, high melting point and photochemical stability.[14–16] The Y^{3+} ions of yttrium oxide crystal are six-fold coordinated to nearest O^{2-} ligands, forming a $[YO_6]^{9-}$ local unit with C_2 site symmetry.[17] After being doped with appropriate rare-earth ions, Y_2O_3 crystals can serve as excellent laser host materials because of their high thermal conductivity and low phonon energy.[18] In recent years, Ho^{3+}-doped Y_2O_3 (Y_2O_3 : Ho) crystal has been the subject of intensive investigations as a great promising laser material.[19] Laversenne *et al.* first demonstrated the growth of Ho^{3+}-doped Y_2O_3 single crystal by using the Laser Heated Pedestal Growth (LHPG) technique.[20] In addition, they especially analyzed the dynamical laser resonant characteristics of Y_2O_3 : Ho. Qin *et al.* studied the luminescence spectra of Ho^{3+}-doped Y_2O_3 under the excitation of a 532 nm continuous-wave laser.[21] The results indicate that Ho^{3+} ion possesses several fluorescence transitions in the ultraviolet and violet region (306, 390 and 428 nm) which are assigned to the transitions of $^3D_3 \rightarrow {}^5I_8$, $^5G_4 \rightarrow {}^5I_8$ and $^5G_5 \rightarrow {}^5I_8$, respectively. Wang *et al.* reported a high output laser operation at around 2.1 μm of Y_2O_3 : Ho with low scattering loss and excellent optical quality.[22] Their results revealed that Ho^{3+}-doped Y_2O_3 system shows attractive prospect in high-power and efficient laser applications as a laser gain medium. Although numerous investigations have been widely reported on Y_2O_3 : Ho, there is no systematic study to elucidate its microstructure and electronic properties.

In this paper, we perform extensive structure searches to obtain the ground-state structure of Y_2O_3 : Ho based on the CALYPSO (Crystal structure AnaLYsis by Particle Swarm Optimization)[23–27] method coupled with the DFT (density functional theory). Furthermore, we calculate and analyze the band structure, density of states and the ELF (electron localized

[a]School of Physical Science and Technology, Southwest University, Chongqing 400715, China. E-mail: zhongmm@swu.edu.cn; xiaotianwang@swu.edu.cn
[b]Department of Physics and Optoelectronic Engineering, Yangtze University, Jingzhou 434023, China. E-mail: zcz19870517@163.com
[c]School of Science, Chongqing University of Posts and Telecommunications, Chongqing 400065, China

function) to gain deeper insights into the electronic properties of Ho^{3+}-doped Y_2O_3 system. The outline of this paper is organized as follows. We exhibit a brief description of the calculation method in Section 2. In Section 3, we present our results and discussion. A conclusion is finally given in Section 4.

2. Computational methods

We have explored the structural evolution of Y_2O_3 : Ho crystal by using the unbiased CALYPSO[23–27] method. The CALYPSO is a reliable structure prediction method which has been validated by a large variety of crystal structures.[28–32] We perform an evolutionary variable-cell structure prediction with 80 atoms per simulation cell at ambient pressure. To determine the most stable structure of Y_2O_3 : Ho system, we optimized the all lowest-lying candidate structures by using the density functional theory in VASP (Vienna *Ab Initio* Simulation Package) code.[33–35] The frozen-core all electron projector-augmented wave (PAW) method has been adopted, with $4f^{11}5s^25p^66s^2$, $4d^15s^2$ and $2s^22p^4$ treated as valence electrons for Ho, Y and O, respectively. For describing the influence of the correlation effect introduced by 4f electrons of Ho atoms, we employ the local density approximation (LDA) with an onsite Coulomb repulsion parameter U[36] to determine the electronic band structure of Y_2O_3 : Ho. The U value of Ho has been determined to be 6.8 eV by Min *et al.*[37] Phonon dispersion curve have been calculated by the PHONOPY code.[38]

3. Results and discussion

We carefully examine the ground-state crystal structure of Ho^{3+}-doped Y_2O_3 by using the unbiased CALYPSO structure search method with the stoichiometric ratio of Ho : Y : O = 1 : 31 : 48 under ambient conditions. The lowest-energy structure of Y_2O_3 : Ho is successfully identified and displayed in Fig. 1. It can be seen from Fig. 1 that the ground-state Y_2O_3 : Ho crystal possesses the monoclinic configuration with the Ho^{3+} ion (0.901 Å) substitute for Y^{3+} ion (0.900 Å) in the Y_2O_3 host. The concentration of the impurity Ho^{3+} is equal to 3.125%, which is in excellent agreement with the result measured by Atabaev *et al.*[15] The site symmetry of $[HoO_6]^{9-}$ local structure are calculated to be C_2 and Ho^{3+} position are six-coordinated by oxygen atoms. The three different bond lengths between Ho–O bonds are calculated to be 2.214, 2.232, and 2.318 Å, respectively. The Ho^{3+} doped Y_2O_3 crystal structure belongs to the standardized $P2$ symmetry and the calculated lattice constants are $a = b = c = 10.524$ Å, $\beta = 90°$. The coordinates of all atoms for the ground state Y_2O_3 : Ho are summarized in Table 1 for further investigations. Moreover, our structure searches also predict many metastable structures of Ho^{3+}-doped Y_2O_3 which can play important roles to explore the structural evolutions. The first four optimized low-lying structures (a), (b), (c) and (d)

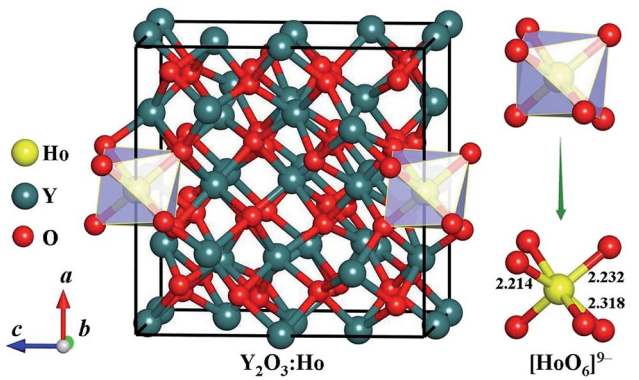

Fig. 1 Crystal structure and $[HoO_6]^{9-}$ local unit of the ground-state Ho^{3+}-doped Y_2O_3. The bond lengths are in the unit of Å.

Table 1 Coordinates of all atoms for the ground state Ho^{3+}-doped Y_2O_3

Atom	x	y	z	Wyckoff site symmetry
Ho	0.50000	0.03244	−0.00000	1c
O(1)	−0.09805	0.37926	0.39177	2e
O(2)	0.40264	0.87998	0.89255	2e
O(5)	0.40205	0.12070	0.60831	2e
O(6)	−0.09818	0.62076	0.10808	2e
O(9)	0.14194	0.15190	0.37921	2e
O(10)	0.64186	0.65190	0.87934	2e
O(11)	−0.14176	0.84802	0.87927	2e
O(12)	0.35819	0.34791	0.37925	2e
O(17)	0.12928	0.39175	0.15192	2e
O(18)	0.62931	0.89190	0.65180	2e
O(19)	0.62868	0.10740	0.84899	2e
O(20)	0.12931	0.60822	0.34801	2e
O(25)	0.59794	0.62079	0.60830	2e
O(26)	0.09816	0.12070	0.10813	2e
O(29)	0.09808	0.87932	0.39175	2e
O(30)	0.59805	0.37924	0.89184	2e
O(33)	0.35820	0.84806	0.62099	2e
O(34)	−0.14195	0.34792	0.12077	2e
O(35)	0.64100	0.15153	0.12014	2e
O(36)	0.14182	0.65199	0.62075	2e
O(41)	0.37080	0.60848	0.84803	2e
O(42)	−0.12934	0.10816	0.34796	2e
O(43)	−0.12943	0.89189	0.15191	2e
O(44)	0.37080	0.39172	0.65211	2e
Y(1)	0.00004	0.24998	0.24998	2e
Y(2)	0.49982	0.75036	0.24967	2e
Y(3)	0.50011	0.24976	0.75024	2e
Y(4)	0.00005	0.75003	0.75003	2e
Y(9)	−0.25020	0.24979	0.96795	2e
Y(10)	−0.25006	0.75002	0.53211	2e
Y(13)	0.71753	0.00010	0.24967	2e
Y(15)	−0.21791	0.50004	0.24995	2e
Y(21)	−0.25026	0.75030	0.03217	2e
Y(22)	0.25002	0.24997	0.53226	2e
Y(25)	−0.21803	0.00001	0.75019	2e
Y(26)	0.28218	0.49999	0.24999	2e
Y(17)	0.00000	0.96781	0.00000	1a
Y(30)	0.00000	0.46784	0.00000	1a
Y(18)	0.50000	0.53219	−0.00000	1c
Y(19)	0.00000	0.03214	0.50000	1b
Y(29)	0.00000	0.53220	0.50000	1b
Y(20)	0.50000	0.46778	0.50000	1d
Y(31)	0.50000	0.96786	0.50000	1d

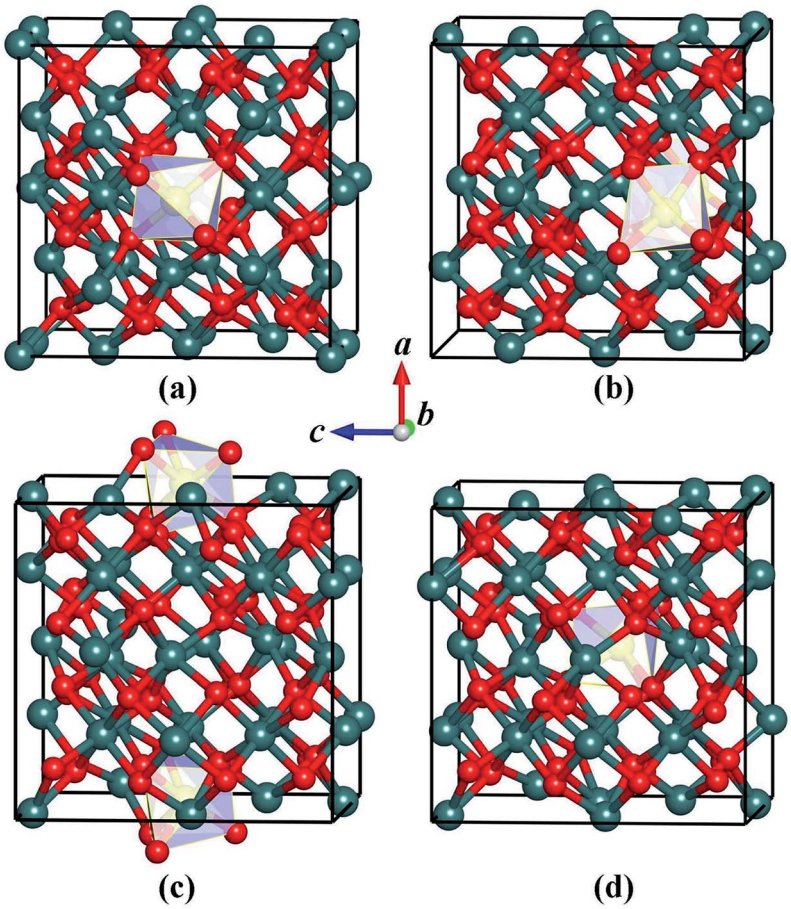

Fig. 2 Coordination structures of the metastable (a–d) for Y_2O_3 : Ho.

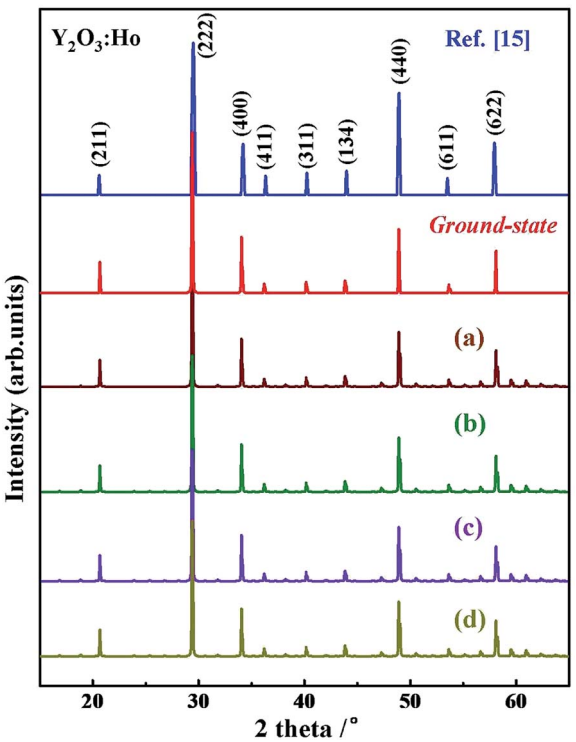

Fig. 3 Comparison of the simulated XRD spectrum for the ground-state and metastable (a–d) Y_2O_3 : Ho with experimental patterns.

from low to high energy are exhibited in Fig. 2. It is found that the Y^{3+} ions of these isomers are replaced by Ho^{3+} ions at different sites in the host crystals. Interestingly, the isomer (a) possesses the same *P*2 monoclinic configuration with the ground-state structure while the isomers (b), (c) and (d) exhibit the *P*1 space group. In these metastable structures, we find that the impurity Ho^{3+} ions tend to occupy the crystal face site positions of the Y^{3+}.

To clarify the true structure of the ground-state Y_2O_3 : Ho, as shown in Fig. 3, we calculate the X-ray diffraction (XRD) patterns of the ground state structure. We can clearly see from Fig. 3 that the simulated spectrum of Y_2O_3 : Ho are in good accordance with the observations in experiment.[15] In addition, the XRD patterns of the four metastable structures are calculated and the results are also plotted in Fig. 3. It can be seen from Fig. 3 that the overall distribution of the peaks is similar, suggesting that the structural parameters of the four metastable structures are close to each other. To further validate the dynamical stability of Ho^{3+}-doped Y_2O_3 system, we have calculated the phonon dispersion curves in Fig. 4 and no imaginary phonon frequencies can be seen over the entire Brillouin zones. The result indicates that the determined ground-state structure of Ho^{3+}-doped Y_2O_3 crystal is dynamically stable. These theoretical results provide great support for the reliability of our structural prediction methodology.

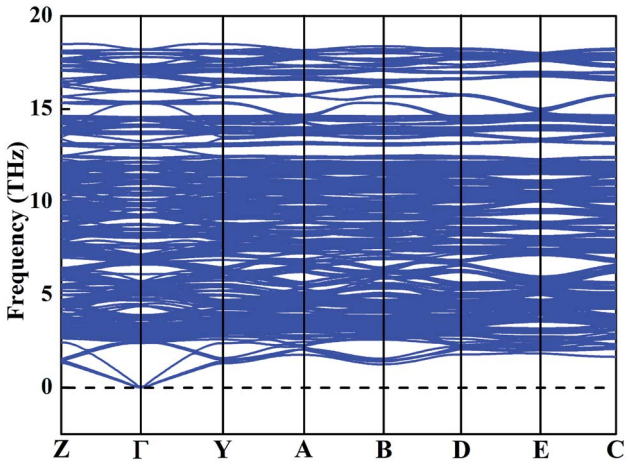

Fig. 4 Calculated phonon dispersion curve for the ground-state Y_2O_3 : Ho.

We have calculated the electronic band structure and the total as well as partial DOS for Y_2O_3 : Ho. As illustrated in Fig. 5(a), the direct band gap value for Ho^{3+}-doped Y_2O_3 is about 4.27 eV at the Γ point, which is approximately 2/3 of the experimental value (E_g = 6.2 eV) determined by Wallace and

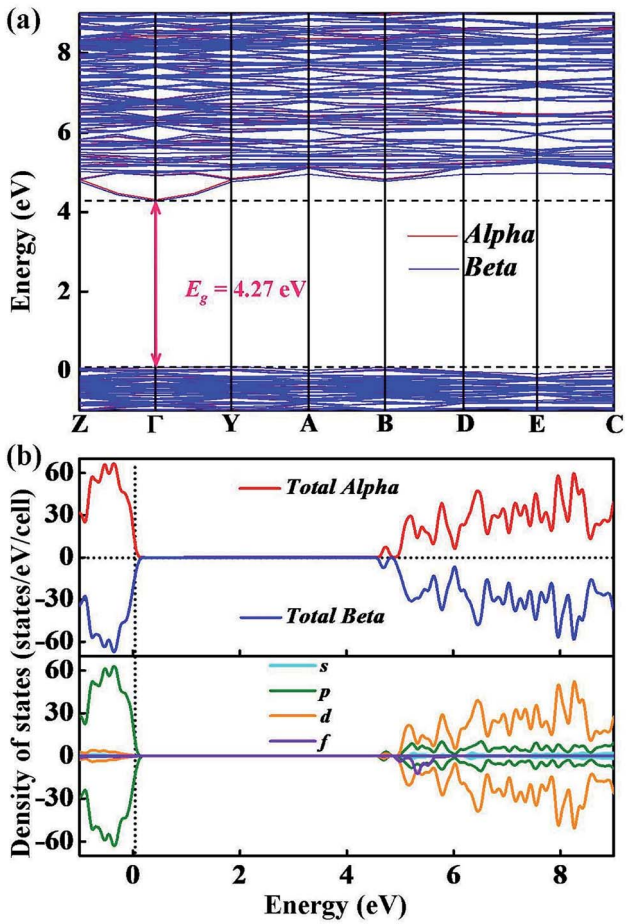

Fig. 5 The calculated (a) electronic band structure and (b) total as well as partial densities of states of Y_2O_3 : Ho.

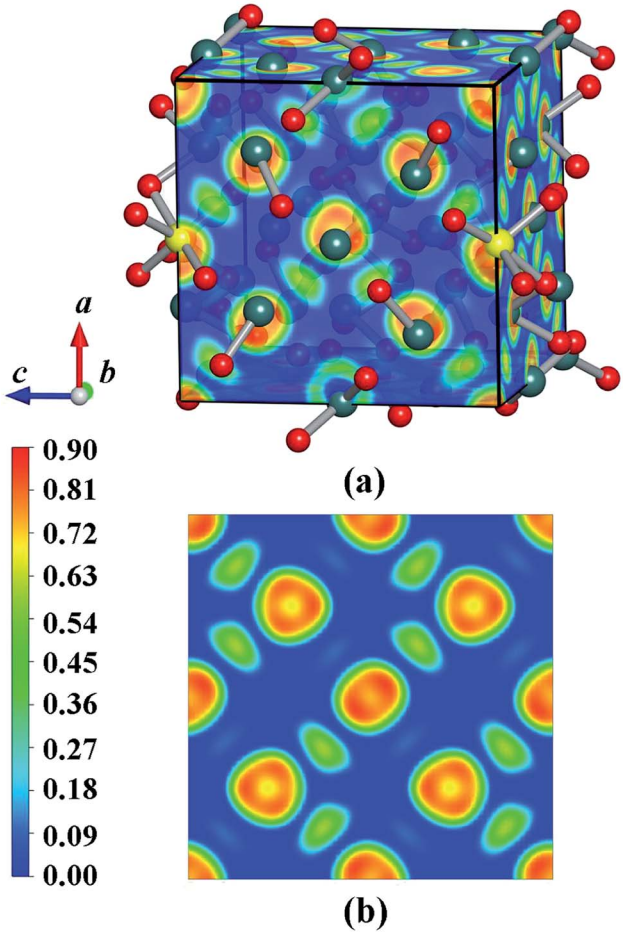

Fig. 6 ELF maps of (a) the structure and (b) ⟨100⟩ plane for the ground-state Y_2O_3 : Ho.

Wilk.[39] This result can be ascribed to the general underestimation of band gap value by the first-principle calculations. The result indicates that the Ho^{3+} impurity ion remains the insulating character of Ho^{3+}-doped Y_2O_3 crystal. From Fig. 5(b), we can clearly see that the low valence band region is mainly composed of p states with the smaller contributors of d states ranging from −1 eV to 0 eV, and the dominant contributions of the high conduction band between 4.3 eV to 9 eV are mainly occupied by p, d and f states. It should be noted that the s states is very weak from −1 eV to 9 eV. In addition, we have calculated the electron localized function (ELF) to visualize the chemical bonding character in Y_2O_3 : Ho crystal. The ELF in crystal structure and the ELF of the (100) plane are presented in Fig. 6. It is shown that the ELF near the Y and Ho atoms value is close to 0.9, which suggests that the electrons are extremely localized around the Y and Ho atoms.

4. Conclusions

In summary, we have explored the ground-state crystal structure of Ho^{3+}-doped Y_2O_3 by means of the unbiased CALYPSO method combined with first-principle calculations. It is shown that the ground-state Y_2O_3 : Ho structure possesses a novel *P*2

phase with the monoclinic symmetry. We carry out a systematical investigation to the microstructure evolutions for the ground-state Y_2O_3 : Ho crystal. The results indicate that the impurity Ho^{3+} ion substitutes the positions of Y^{3+} ions in the host crystal lattice, forming the $[HoO_6]^{9-}$ local structure. We find that the impurity Ho^{3+} ions tend to occupy the crystal face positions of the Y^{3+} ions from the structural features of the ground-state and metastable structures. We further calculate the band structure and density of states by LDA + *U* method for Y_2O_3 : Ho. Our result reveals that the electronic band gap of Ho^{3+}-doped Y_2O_3 is 4.27 eV. We hope that these findings can provide valuable guidance for future experiment research of Y_2O_3 : Ho.

Conflicts of interest

The authors declare no competing interests.

Acknowledgements

This work is supported by the National Natural Science Foundation of China (No. 11904297, 11747139 and 11804031) and the Fundamental Research Funds for the Central Universities (SWU118055), the Scientific Research Project of Education Department of Hubei Province (No. Q20191301), the Youth Fund of Yangtze University (No. 2016cqn, Y. Y. J.).

References

1 P. S. J. Bharadwaj, S. Kundu, V. S. Kollipara and K. B. R. Varma, Synergistic effect of trivalent (Gd^{3+}, Sm^{3+}) and high-valent (Ti^{4+}) co-doping on antiferromagnetic $YFeO_3$, *RSC Adv.*, 2020, **10**, 22183–22195.

2 J. Bai, P. Duan, X. Wang, G. Han, M. Wang and G. Diao, Upconversion luminescence enhancement by Fe^{3+} doping in CeO_2 : Yb/Er nanomaterials and their application in dye-sensitized solar cells, *RSC Adv.*, 2020, **10**, 18868–18874.

3 Monika, R. S. Yadav, A. Bahadur and S. B. Rai, Concentration and pump-mediated color tenability, optical heating and temperature sensing *via* TCLs of red emission in an Er^{3+}/Yb^{3+}/Li^{+} co-doped $ZnGa_2O_4$ phosphor, *RSC Adv.*, 2019, **9**, 40092–40108.

4 N. Choudhary, M. K. Verma, N. D. Sharma, S. Sharma and D. Singh, Correlation between magnetic and transport properties of rare earth doped perovskite manganites $La_{0.6}R_{0.1}Ca_{0.3}MnO_3$ (R = La, Nd, Sm, Gd, and Dy) synthesized by Pechini process, *Mater. Chem. Phys.*, 2020, **242**, 122482.

5 M. P. Ghosh, S. Sharma, H. K. Satyapal, K. Tanbir, R. K. Singh and S. Mukherjee, Tuning the microstructural, optical and superexchange interactions with rare earth Eu doping in nickel ferrite nanoparticles, *Mater. Chem. Phys.*, 2020, **241**, 122383.

6 S. D. Jackson, Towards high-power mid-infrared emission from a fibre laser, *Nat. Photonics*, 2012, **6**, 423–431.

7 I. Cieslik, T. Bolek, M. J. Wozniak, A. Majchrowski, S. Hirano and A. Budzianowski, Potassium gadolinium tungstate nanocrystals doped with holmium ions as candidates for optical imaging, *Appl. Surf. Sci.*, 2018, **446**, 139–144.

8 Y. R. Fang and M. T. Sun, Nanoplasmonic waveguides: towards applications in integrated nanophotonic circuits, *Light: Sci. Appl.*, 2015, **4**, e294.

9 X. Y. Wang, Y. L. Wang, S. Wang, B. Li, X. W. Zhang, L. Dai and R. M. Ma, Lasing Enhanced Surface Plasmon Resonance Sensing, *Nanophotonics*, 2017, **6**, 472–478.

10 A. Z. Li, M. Zhang, X. Wang, S. B. Wang, B. G. Guo, E. Lewis and P. F. Wang, Directly pumped Ho^{3+}-doped microspheres lasing at 2.0 μm, *IEEE Photonics Technol. Lett.*, 2019, **31**, 1366–1368.

11 S. Balaji, G. Gupta, K. Biswas, D. Ghosh and K. Annapurna, Role of Yb^{3+} ions on enhanced ~2.9 μm emission from Ho^{3+} ions in low phonon oxide glass system, *Sci. Rep.*, 2016, **6**, 29203.

12 M. Eichhorn, Quasi-three-level solid-state lasers in the near and mid infrared based on trivalent rare earth ions, *Appl. Phys. B*, 2008, **93**, 269–316.

13 M. C. Pujol, J. Massons, M. Aguiló, F. Díaz, M. Rico and C. Zaldo, Emission Cross Sections and Spectroscopy of Ho^{3+} Laser Channels in $KGd(WO_4)_2$ Single Crystal, *IEEE J. Quantum Electron.*, 2002, **38**, 93–100.

14 A. Ciric and S. Stojadinovic, Structural and photoluminescence properties of Y_2O_3 and Y_2O_3 : Ln^{3+} (Ln = Eu, Er, Ho) films synthesized by plasma electrolytic oxidation of yttrium substrate, *J. Lumin.*, 2020, **217**, 116762.

15 T. S. Atabaev, H. H. T. Vu, Y. D. Kim, J. H. Lee, H. K. Kim and Y. H. Hwang, Synthesis and luminescence properties of Ho^{3+} doped Y_2O_3 submicron particles, *J. Phys. Chem. Solids*, 2012, **73**, 176–181.

16 B. M. Walsh, J. M. McMahon, W. C. Edwards, N. P. Barnes, R. W. Equall and R. L. Hutcheson, Spectroscopic characterization of Nd : Y_2O_3: application toward a differential absorption lidar system for remote sensing of ozone, *J. Opt. Soc. Am. B*, 2002, **19**, 2893–2903.

17 M. Ju, Y. Xiao, W. G. Sun, C. Lu and Y. Y. Yeung, In-depth determination of the microstructure and energy transition mechanism for Nd^{3+}-doped yttrium oxide laser crystals, *J. Phys. Chem. C*, 2020, **124**, 2113–2119.

18 V. Singh, V. K. Rai, B. Voss, M. Haase, R. P. S. Chakradhar, D. T. Naidu and S. H. Kim, Photoluminescence study of nanocrystalline Y_2O_3 : Ho^{3+} phosphor, *Spectrochim. Acta, Part A*, 2013, **109**, 206–212.

19 G. A. Newburgh, A. W. Daniels, A. Michael, L. D. Merkle, A. Ikesue and M. Dubinskii, Resonantly diode-pumped Ho^{3+} : Y_2O_3 ceramic, *Opt. Express*, 2011, **19**, 3604–3611.

20 L. Laversenne, C. Goutaudier, Y. Guyot, M. T. Cohen-Adad and G. Boulon, Growth of rare earth (RE) doped concentration gradient crystal fibers and analysis of dynamical processes of laser resonant transitions in RE-doped Y_2O_3 (RE = Yb^{3+}, Er^{3+}, Ho^{3+}), *J. Alloys Compd.*, 2002, **341**, 214–219.

21 F. Qin, Y. D. Zheng, Y. Yu, Z. M. Chen, P. S. Tayebi, W. W. Cao and Z. G. Zhang, Ultraviolet and violet upconversion luminescence in Ho^{3+}-doped Y_2O_3 ceramic

induced by 532-nm CW laser, *J. Alloys Compd.*, 2011, **509**, 1115–1118.

22 F. Wang, J. W. Tang, E. H. Li, C. F. Shen, J. Wang, D. Y. Tang and D. Y. Shen, $Ho^{3+}:Y_2O_3$ ceramic laser generated over 113 W of output power at 2117 nm, *Opt. Lett.*, 2019, **44**, 5933–5936.

23 Y. C. Wang, J. Lv, L. Zhu and Y. M. Ma, Crystal structure prediction *via* particle-swarm optimization, *Phys. Rev. B: Condens. Matter Mater. Phys.*, 2010, **82**, 094116.

24 Y. C. Wang, J. Lv, L. Zhu and Y. M. Ma, CALYPSO: a method for crystal structure prediction, *Comput. Phys. Commun.*, 2012, **183**, 2063–2070.

25 Y. C. Wang, M. S. Miao, J. Lv, L. Zhu, K. T. Yin, H. Y. Liu and Y. M. Ma, An effective structure prediction method for layered materials based on 2D particle swarm optimization algorithm, *J. Chem. Phys.*, 2012, **137**, 224108.

26 S. H. Lu, Y. C. Wang, H. Y. Liu, M. S. Miao and Y. M. Ma, Self-assembled ultrathin nanotubes on diamond (100) surface, *Nat. Commun.*, 2014, **5**, 3666.

27 L. Zhu, H. Y. Liu, C. J. Pickard, G. T. Zou and Y. M. Ma, Reactions of xenon with iron and nickel are predicted in the Earth's inner core, *Nat. Chem.*, 2014, **6**, 644–648.

28 J. Lv, Y. C. Wang, L. Zhu and Y. M. Ma, Particle-swarm structure prediction on clusters, *J. Chem. Phys.*, 2012, **137**, 084104.

29 Y. Xiao, M. Ju, X. Y. Kuang and Y. Y. Yeung, A systematic study of the microstructure and laser characteristics of Pr^{3+}-doped lithium lutetium fluoride, *J. Alloys Compd.*, 2018, **749**, 391–398.

30 G. Bo, P. Gao, S. Lu, J. Lv, Y. Wang and Y. Ma, Interface structure prediction *via* CALYPSO method, *Sci. Bull.*, 2019, **64**, 301.

31 C. Lu and C. Chen, Indentation-strain stiffening in tungsten nitrides: mechanisms and implications, *Phys. Rev. Mater.*, 2020, **4**, 043402.

32 C. Lu and C. Chen, Structure-strength relations of distinct MoN phases from first-principles calculations, *Phys. Rev. Mater.*, 2020, **4**, 044002.

33 G. Kresse and J. Furthmüller, Efficient iterative schemes for *ab initio* total-energy calculations using a plane-wave basis set, *Phys. Rev. B: Condens. Matter Mater. Phys.*, 1996, **54**, 11169–11186.

34 G. Kresse and J. Hafner, *Ab initio* molecular dynamics for liquid metals, *Phys. Rev. B: Condens. Matter Mater. Phys.*, 1993, **47**, 558–561.

35 J. P. Perdew, K. Burke and M. Ernzerhof, Generalized gradient approximation made simple, *Phys. Rev. Lett.*, 1996, **77**, 3865–3868.

36 V. I. Anisimov, F. Aryasetiawan and A. I. Lichtenstein, First-principles calculations of the electronic structure and spectra of strongly correlated systems: the LDA + *U* Method, *J. Phys.: Condens. Matter*, 1997, **9**, 767–808.

37 B. I. Min, H. J. F. Jansen, T. Oguchi and A. J. Freeman, Local density total energy description of ground and excited state properties of the rare earth metals, *J. Magn. Magn. Mater.*, 1986, **61**, 139–150.

38 A. Togo, F. Oba and I. Tanaka, First-principles calculations of the ferroelastic transition between rutile-type and $CaCl_2$-type SiO_2 at high pressures, *Phys. Rev. B: Condens. Matter Mater. Phys.*, 2008, **78**, 134106.

39 R. M. Wallace and G. Wilk, Alternative gate dielectrics for microelectronics, *Bulletin*, 2002, **27**, 186.